Article

JFPE

Journal of Fire Protection Engineering
23(3) 177–189

DOI: 10.1177/1042391512472498
jfe.sagepub.com

SAGE

A numerical model for concrete slabs under fire conditions

Rodrigo Berreto Caldas and Ricardo Hallal Fakury
Department of Structural Engineering, Federal University of Minas Gerais, Minas Gerais, Brazil

Joao Batista Marques Sousa Jr
Department of Civil Engineering, Federal University of Ouro Preto, Minas Gerais, Brazil

Roque Luiz da Silva Pitanqueira
Department of Structural Engineering, Federal University of Minas Gerais, Minas Gerais, Brazil

Abstract
A numerical model for the behavior of concrete slabs in a fire is described. This model consists of a shell finite element, a damage constitutive model for concrete with steel reinforcement and the consideration of heat transfer through the thickness of the slab. An improved damage constitutive model for concrete at elevated temperatures has been implemented considering compressive and tensile behavior through an orthotropic compliance theory. The damage in compression is based on the concrete stress–strain relationships presented by the European Committee for Standardization. Several calculations have been performed to validate the improved model. The comparison with experimental tests and numerical results confirm the validity of the approach for reinforced concrete slabs subjected to large transverse displacement.

Keywords
Structures, fire, finite element, slab, concrete, damage

Corresponding author:
Rodrigo Berreto Caldas, Department of Structural Engineering, Federal University of Minas Gerais, Minas Gerais, Brazil.
Email: caldas@dees.ufmg.br

Introduction

Fires and fire tests [1–4] have confirmed that steel members in real multistorey buildings have significantly greater fire resistance than isolated members in the standard fire test. One reason for this is the membrane action in the structure under fire conditions. Both numerical and analytical models have been developed by many researchers to better understand the fire behavior of concrete slabs as well. A review of some of the latter work is described below.

Nizamuddin [5] developed a nonlinear layered finite element approach based on the Kirchhoff (thin plate) theory to model reinforced concrete slabs under fire conditions.

Bailey [6] utilized the Mindlin/Reissner (thick plate) theory in order to develop a model for concrete slabs in steel and composite buildings using the VULCAN program. Huang et al. [7] implemented nonlinear shell elements subdivided into layers which represented concrete and steel reinforcement. A smeared crack model was adopted with a failure criterion surface. After cracking, the concrete is treated as an orthotropic material with principal axes normal and parallel to the crack direction. Huang et al. [8,9] considered geometric nonlinearity based on the hypotheses of von Kármán and an effective-stiffness factor adopted to modify the material stiffness matrices in order to take into account the orthotropic properties of composite slabs.

Lim et al. [10,11] describe the numerical modeling of the fire behavior of reinforced concrete slabs using the SAFIR program. The four node shell element presented is based on the Discrete Kirchhoff Quadrilateral (DKQ) and includes membrane properties. A corotational configuration is adopted [12]. The concrete properties are modeled using a temperature dependent von Mises plane stress associated plasticity model with a Rankine cut off under tensile stress [13].

Elghazouli et al. [14,15] use a grillage representation of the building floor in the ADAPTIC program. Gillie et al. [16] model composite floor slabs under fire conditions using a stress-resultant approach. The modeling is performed using the Finite Element Analysis of Shells at High Temperatures (FEAST), a suite of programs developed for the analysis of orthotropic plates and also designed to interact with the commercial finite element program, ABAQUS.

Simple design methods [17,18] have been developed to take into account membrane action in concrete or composite steel and concrete slabs. The design method presented by Newman et al. [17] has subsequently been updated [1,19] to include more efficient reinforcement patterns and the practical use of natural fires. Recently, other updates have been made with the aid of the results of the research programs FRACOF, MACS+ and FICEB+ [2–4].

Tenchev and Purnel [20] present a damage model capable of evaluating concrete spalling. The model considers the interaction between the aggregate and the mortar as well as the prediction of the stress involved in spalling effects. References to other models for concrete at high temperature based on plasticity, damage, or a combination of the two, are also presented by the authors.

This article presents a finite element model for concrete slabs under fire conditions. A damage model for concrete at elevated temperatures has been adopted considering compressive and tensile behavior through an orthotropic compliance theory. The damage in compression is based on the concrete stress–strain relationships presented by Eurocode 2 [21]. This work has been carried out in order to analyze a smaller, isolated structure, free from interactions with the surrounding structure, with the intention of concentrating on the advancement of the damage model for concrete at elevated temperatures.

The implementation and verification of the damage model and shell element were performed by Caldas [22] in the FEMOOP-FIRE program, written in the C++ programming language. The program was developed by Caldas [22] based on a previously existing program [23] used in other studies by Sousa Jr. and Caldas [24]. Three-dimensional beam elements, shell and spring elements, for modeling steel, concrete and composite structures in a fire, were developed [22]. The damage constitutive model, implemented in the FEMOOP-FIRE program and described in the next section, has the significant advantage of using the complete stress–strain relationship for concrete, which differs from other models that are based on failure surfaces and plasticity [13,25].

Damage constitutive model

The damage model presented is based on a generalization of the Bazant and Oh work [26] in such a way that it considers both tensile and compressive damage. A complete explanation of the model and background information can be viewed at Pitangueira [27]. The extension to concrete at elevated temperatures presented here was developed by Caldas [22]. The model assumes the validity of the stress–strain compliance relationship

$$\boldsymbol{\varepsilon}_{12} = \mathbf{D}\boldsymbol{\sigma}_{12}, \tag{1}$$

where $\mathbf{D}$ is the constitutive compliance matrix, $\boldsymbol{\varepsilon}_{12}$ the strain vector associated with the plane stress vector $\boldsymbol{\sigma}_{12}$ in the local system of axes (1, 2) defined along with the principal axes of orthotropy. Axis 1 is the largest principal strain direction (most positive) and axis 2 is the minor principal strain (tensile strains are positive and compressive strains negative). These axes are fixed for each step (load increment or time increment of fire exposure) in the Newton Raphson method, which is used to solve the system of nonlinear equations that represent the model.

To obtain a symmetric compliance matrix, an assumption for the coupling due to the Poisson effect should be adopted. The hypothesis most widely used is that the coupling is given by the initial modulus of the material before damage, E_0, and by a

single value of Poisson's ratio, ν, valid for any direction. Therefore, for the plane stress state, the constitutive compliance matrix is

$$\mathbf{D} = \begin{bmatrix} \frac{1}{E_1} & -\frac{\nu}{E_0} & 0 \\ -\frac{\nu}{E_0} & \frac{1}{E_2} & 0 \\ 0 & 0 & \frac{1}{G_{12}} \end{bmatrix}, \tag{2}$$

which, when inverted, leads to the constitutive secant stiffness matrix

$$\mathbf{C}_{12}^{s} = \frac{1}{1 - \frac{E_1 E_2}{E_0^2}\nu^2} \begin{bmatrix} E_1 & \frac{\nu E_1 E_2}{E_0} & 0 \\ \frac{\nu E_1 E_2}{E_0} & E_2 & 0 \\ 0 & 0 & \left(1 - \frac{E_1 E_2}{E_0^2}\nu^2\right) G_{12} \end{bmatrix}, \tag{3}$$

where E_1 and E_2 are the secant modules obtained from the adopted damage law and the strain which occurs in each direction, respectively. For compressive strains, secant modules are obtained from the stress–strain relationship given by Eurocode 2 [21] for concrete at elevated temperatures. For tensile strains, the stress–strain relationship, presented by Huang et al. [8], is adopted with a reduction factor for tensile strength taken equal to the reduction factor for compressive strength raised to the third power [22].

Talamona and Franssen [13] discuss the influence of tensile strength on behavior of slabs subjected to fire, and Lim et al. [10] comment that the displacement predictions for slabs with light steel reinforcement were sensitive to the concrete tensile strength. The stress–strain and reduction factors adopted in this work have been adequate.

The unloading of the model follows the secant modulus which indicates that the maximum damage level is fixed. This hypothesis also simulates the behavior of the cold concrete after a fire that does not recover its initial strength [21].

The transverse modulus given by

$$G_{12} = \frac{E_0 E_1 E_2}{E_0 E_1 + E_0 E_2 + 2\nu E_1 E_2}, \tag{4}$$

appearing in equations (2) and (3) shall be limited by $G_{12} \geq \beta G_0$, where G_0 is the initial transverse modulus of elasticity and β is a retention factor taken as 0.25.

Total stress is given by

$$\boldsymbol{\sigma}_{12} = \mathbf{C}^{s}_{12}\boldsymbol{\varepsilon}_{12}. \tag{5}$$

where $\boldsymbol{\varepsilon}_{12}$ is an effective deformation equal to the total strain (function of the displacements of the structure) minus the thermal strain [28].

The constitutive tangent stiffness matrix in equation (6)

$$\mathbf{C}^{t}_{12} = \frac{\partial \boldsymbol{\sigma}_{12}}{\partial \boldsymbol{\varepsilon}_{12}}, \tag{6}$$

can be obtained by differentiating equation (5), which then becomes:

$$\mathbf{C}^{t}_{12} = \frac{\partial \boldsymbol{\sigma}_{12}}{\partial \boldsymbol{\varepsilon}_{12}} = \frac{\partial}{\partial \boldsymbol{\varepsilon}_{12}}\left(\mathbf{C}^{t}_{12}\boldsymbol{\varepsilon}_{12}\right) = \mathbf{C}^{s}_{12} + \frac{\partial \mathbf{C}^{s}_{12}}{\partial \boldsymbol{\varepsilon}_{12}}\boldsymbol{\varepsilon}_{12}. \tag{7}$$

In equation (7), the term $\frac{\partial \mathbf{C}^{s}_{12}}{\partial \boldsymbol{\varepsilon}_{12}}\boldsymbol{\varepsilon}_{12}$ given by

$$\frac{\partial \mathbf{C}^{s}_{12}}{\partial \boldsymbol{\varepsilon}_{12}}\boldsymbol{\varepsilon}_{12} = \begin{bmatrix} \dfrac{\partial C^{s}_{11}}{\partial \varepsilon_1}\varepsilon_1 + \dfrac{\partial C^{s}_{12}}{\partial \varepsilon_1}\varepsilon_2 & \dfrac{\partial C^{s}_{11}}{\partial \varepsilon_2}\varepsilon_1 + \dfrac{\partial C^{s}_{12}}{\partial \varepsilon_2}\varepsilon_2 & 0 \\ \dfrac{\partial C^{s}_{12}}{\partial \varepsilon_1}\varepsilon_1 + \dfrac{\partial C^{s}_{22}}{\partial \varepsilon_1}\varepsilon_2 & \dfrac{\partial C^{s}_{12}}{\partial \varepsilon_2}\varepsilon_1 + \dfrac{\partial C^{s}_{22}}{\partial \varepsilon_2}\varepsilon_2 & 0 \\ 0 & 0 & 0 \end{bmatrix}, \tag{8}$$

is calculated numerically and, in general, is unsymmetrical. Symmetry is obtained by taking the average of the matrix and its transpose.

In the previous equations, the transformations between the local and global coordinate systems are not presented in order to provide a simpler explanation of the model. These transformations can be seen in Caldas [22].

Steel reinforcement is modeled using equivalent distributed steel layers (Figure 1) with constitutive properties only in the direction of the reinforcement [8], considering the stress–strain relationships given by Eurocode 2 [21]. The equivalent layer can have any orientation in the local plane defined by its local vertical coordinate in the element and the orientation of the reinforcement relative to the global x-axis. Full composite action between the concrete and the reinforcing steel is assumed.

The temperature distribution through the slab, in the thickness direction (see Figure 1), is obtained by a one-dimensional explicit finite difference scheme. The temperature increment Δa in each layer i of the slab, at each time increment, ΔT, is given by

$$\Delta a_i = \frac{\Delta T}{c_{v\,i}\Delta z_i}\sum_{j=1}^{n} q_j, \tag{9}$$

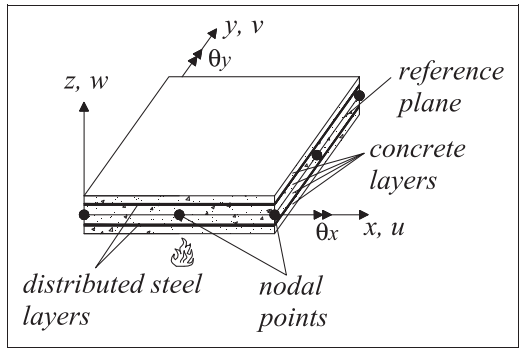

Figure 1. Shell element notation.

where $c_{v\,i}$ is the volumetric specific heat and q_j represents the heat flux between the layer i and the adjacent layers $j = 1, \ldots, n$ and boundary heat flux (convective and radiative) to the contour of slab.

For heat transfer analysis, steel, concrete and fire protection materials are implemented. For concrete, spalling is not considered and moisture content is modeled through the modification of the specific heat according to Eurocode 2 [21].

Finite element formulation

An isoparametric shell element with nine nodal points [29] was adopted in this work. Based on the assumptions of von Kármán, the Green-Lagrange strain vector, as applied to plane stress, is given by

$$\boldsymbol{\varepsilon} = \begin{bmatrix} \varepsilon_x \\ \varepsilon_y \\ \gamma_{xy} \end{bmatrix} = \boldsymbol{\varepsilon}_o + z\mathbf{k} = \begin{bmatrix} \dfrac{\partial u}{\partial x} + \dfrac{1}{2}\left(\dfrac{\partial w}{\partial x}\right)^2 \\ \dfrac{\partial v}{\partial y} + \dfrac{1}{2}\left(\dfrac{\partial w}{\partial y}\right)^2 \\ \dfrac{\partial u}{\partial y} + \dfrac{\partial v}{\partial x} + \dfrac{\partial w}{\partial x}\dfrac{\partial w}{\partial y} \end{bmatrix} + z \begin{bmatrix} \dfrac{\partial \theta_y}{\partial x} \\ \dfrac{-\partial \theta_x}{\partial y} \\ \dfrac{-\partial \theta_x}{\partial x} + \dfrac{\partial \theta_y}{\partial y} \end{bmatrix} \tag{10}$$

where z is the coordinate relative to the reference plane element (vertical direction) and u, v, θ_x and θ_y are displacements and rotations of the reference plane expressed in terms of nodal displacements using quadratic interpolation functions (Figure 1).

The vertical shear strains are given by

$$\boldsymbol{\gamma} = \begin{bmatrix} \gamma_{xz} \\ \gamma_{yz} \end{bmatrix} = \begin{bmatrix} \theta_y \\ -\theta_x \end{bmatrix} + \begin{bmatrix} \dfrac{\partial w}{\partial x} \\ \dfrac{\partial w}{\partial y} \end{bmatrix} = \boldsymbol{\theta} + \mathbf{s} \tag{11}$$

where w is the vertical displacement of the reference plane.

Using the principle of virtual work and considering that $\mathbf{k} = \mathbf{B}_k\mathbf{q}$, $\boldsymbol{\gamma} = \mathbf{B}_\gamma\mathbf{q}$, $\boldsymbol{\varepsilon}_o = \mathbf{B}_\varepsilon\mathbf{q}$ and $\mathbf{s} = \mathbf{B}_s w$, where $\mathbf{q} = \lfloor\, u \quad v \quad w \quad \theta_x \quad \theta_y \,\rfloor$, one can obtain the internal force vector

$$\mathbf{p}_i = \int \left(\mathbf{B}_\varepsilon^T\mathbf{N} + \mathbf{B}_k^T\mathbf{M} + \mathbf{B}_\gamma^T\mathbf{Q}\right) dA_o \tag{12}$$

where $\mathbf{N} = \int \boldsymbol{\sigma} dz$, $\mathbf{M} = \int \boldsymbol{\sigma} z dz$ and $\mathbf{Q} = \int \alpha G \boldsymbol{\gamma}$ are obtained from the sum through the layers, $\boldsymbol{\sigma}$ is the plane stress in the global system obtained from transformation of the local plane stress (equation 5) and α is the 'shear factor', taken as 5/6 for constant thickness.

The tangent stiffness matrix can be obtained from the differentiation of equation (12),

$$\mathbf{k}_i = \int \begin{bmatrix} \mathbf{B}_\varepsilon^T \\ \mathbf{B}_k^T \\ \mathbf{B}_\gamma^T \end{bmatrix} \begin{bmatrix} \mathbf{C}_m & \mathbf{C}_{mb} & \mathbf{0} \\ \mathbf{C}_{mb}^T & \mathbf{C}_b & \mathbf{0} \\ \mathbf{0} & \mathbf{0} & \mathbf{C}_\gamma \end{bmatrix} \begin{bmatrix} \mathbf{B}_\varepsilon \\ \mathbf{B}_k \\ \mathbf{B}_\gamma \end{bmatrix} dA_o + \int \mathbf{B}_s^T \mathbf{N}_2 \mathbf{B}_s dA_o \tag{13}$$

where $\mathbf{N}_2$ are the forces on the reference plane and

$$\mathbf{C}_m = \int \mathbf{C}^t dz,\ \mathbf{C}_{mb} = \int \mathbf{C}^t z dz,\ \mathbf{C}_b = \int \mathbf{C}^t z^2 dz \text{ e } \mathbf{C}_\gamma = \alpha G t \mathbf{I}_2 \tag{14}$$

where t is the slab thickness, $\mathbf{C}^t$ is the constitutive tangent stiffness matrix in the global system obtained from the transformation of the local matrix, equation (6), and $\mathbf{I}_2$ is the 2×2 identity matrix. The integrals in equation (14) are obtained as a sum using the layers of shell thickness [8].

The integration of the internal force vector and stiffness matrix in the area A_o of the element reference plane is performed using the three-point formula of Gauss quadrature. More details can be found in Caldas [22].

Examples

The numerical model developed and implemented in the FEMOOP-FIRE program was tested against various experimental and numerical results.

Concrete slabs at ambient temperature

Ghoneim and MacGregor [30,31] conducted a series of tests on reinforced concrete plates under combined in-plane compressive and lateral loads (i.e., loads perpendicular to the plate). Two specimens denoted B1 and C1, that were tested under

lateral load only, were analyzed by Huang et al. [25] using the VULCAN program. Both plates were simply supported on four edges. Both the top and bottom reinforcement layers were composed of a steel area of 260 mm^2/m in both orthogonal directions.

In the present work, the specimens B1 and C1 are analyzed using the same discretization adopted by Huang et al. [25]. Test B1 was a rectangular plate with dimensions of 2745 mm × 1829 mm and thickness of 68.2 mm. Specimen C1 was a square plate with dimensions of 1829 mm × 1829 mm and thickness of 67.8 mm. The yield stress of steel was assumed to be 450 MPa and the compressive strength of the concrete was 18.7 MPa and 25.2 MPa for specimens B1 and C1, respectively. The finite element was subdivided into 16 layers along the plate thickness.

The predictions of central displacement, together with experimental and VULCAN results, are plotted in Figure 2.

It is observed that the model produces good results in comparison with VULCAN numerical results and fits well with experimental results. Despite the indication that the numerical results lead to a higher ultimate load of failure, it should be noted that the tests terminated before run-away failure occurred.

Small-scale concrete slabs at elevated temperature

Bailey and Toh [19] present a series of tests at ambient and elevated temperatures on horizontally unrestrained small-scale concrete slabs, reinforced with either mild steel or stainless steel mesh reinforcement of different grades, ductility, sizes and reinforcing steel spacing. The fire tests showed compressive and tensile membrane action occurs around the perimeter and at the center of the slabs, respectively. Some fire tests with mild steel (considered hot rolled in the present analysis) were analyzed with the present formulation.

Figure 3 presents the results of Test MF4 with a dimension of 1.15 m × 1.15 m, a thickness of 19.6 mm and reinforcing steel in both directions having a diameter of

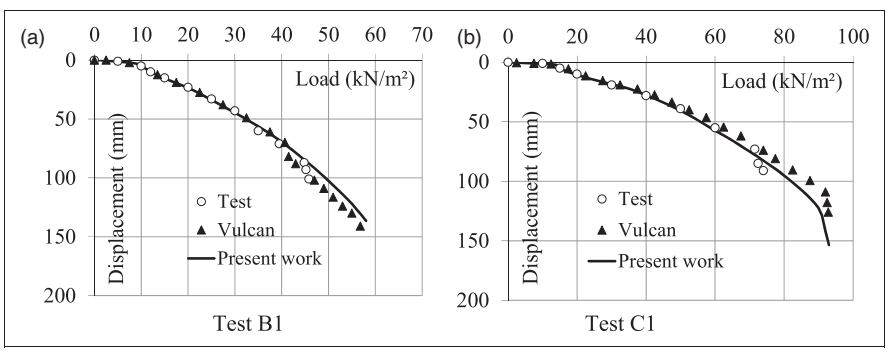

Figure 2. Comparison of central displacements for test B1 and C1.

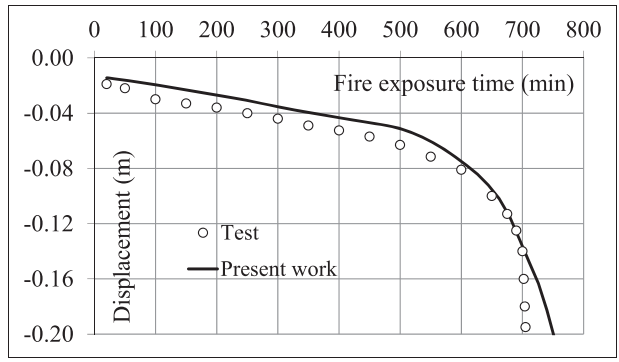

Figure 3. Central displacement of Test MF4.

1.54 mm, a spacing of 25.4 mm and a concrete cover of 5 mm. The strength of concrete was 39 MPa and the yield strength of steel was 311 MPa. The superimposed load of 5.429 kN/m^2 (including self-weight of the slab) was applied and kept constant during the fire exposure time. The slab was divided into 16 finite elements and subdivided into 17 layers. It is observed that the model produces good results in comparison with experimental results.

Restrained concrete slabs at elevated temperature

Lin et al. [32] present the results of a fire test conducted on a full-scale reinforced concrete slab (Test S56) in which expansion was restrained in order to simulate behavior in a real structure. Huang et al. [25] present numerical results for this same Test S56 using the VULCAN program.

The compressive strength of the concrete was considered as 36 MPa and the yield strength of reinforcing steel was 414 MPa. The imposed restraint forces were considered constant during fire exposure and equal to 600 kN and 1200 kN in the directions west and south, respectively. The superimposed uniform applied load, kept constant during fire exposure, was 6.61 kN/m^2. Beam elements [22] with a small torsional stiffness (550 kNm^2) based on cracking concrete properties and minimum steel reinforcement was considered at the edges of the slab. The temperature distribution through the thickness of the slab has been calculated considering a standard fire exposure from the ASTM E119 time-temperature curve. The concrete properties were considered in accordance with the Eurocode 2 [21], taking into account calcareous aggregate, the lower limit for thermal conductivity and a moisture content of 3% by weight. Hot rolled properties for reinforcing steel were considered. The distribution of the reinforcement can be seen in Lin et al. [32]. The reinforcing steel temperature was assumed to be the same as the concrete temperature adjacent to it, as it was neglected in the temperature calculations. The slab thickness was divided into 23 layers.

The central displacements are shown in Figure 4. The numerical results closely follow the experimental results. Like the VULCAN program, this model shows

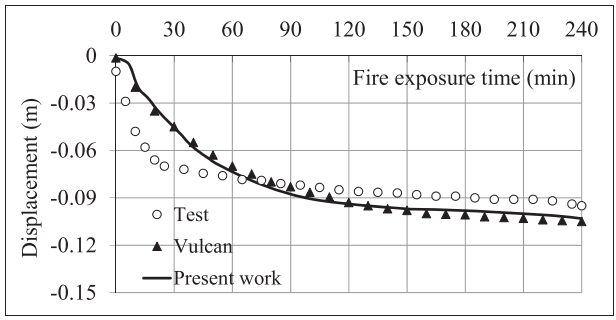

Figure 4. Central displacement of Test S56.

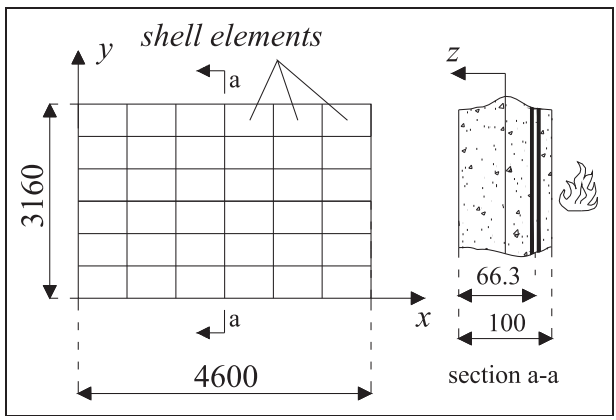

Figure 5. Concrete slab tested by Lim and Wade [33]. Dimensions in mm.

displacements smaller than the experimental ones at the beginning of fire exposure. This may indicate that the temperature distribution along the slab thickness is more severe than that obtained by thermal analysis. The differences between the numerical results should be coupled with restraining forces considered to be constant and the value adopted for the edge beam torsional stiffness.

Unrestrained concrete slabs at elevated temperature

Talamona and Franssen [13] present numerical results obtained with the SAFIR program for the fire test of concrete slab conducted by Lim and Wade [33]. The slab was simply supported at all four edges and axially unrestrained. The superimposed uniform load applied was 3.0 kN/m^2 and was kept constant during standard fire exposure (ISO 834).

Figure 5 shows the dimensions and discretization of the slab. The thickness was 100 mm, the compressive strength of concrete was 36 MPa and the concrete cover was 25 mm. The reinforcing mesh was made of steel bars every 300 mm with 8.7 mm

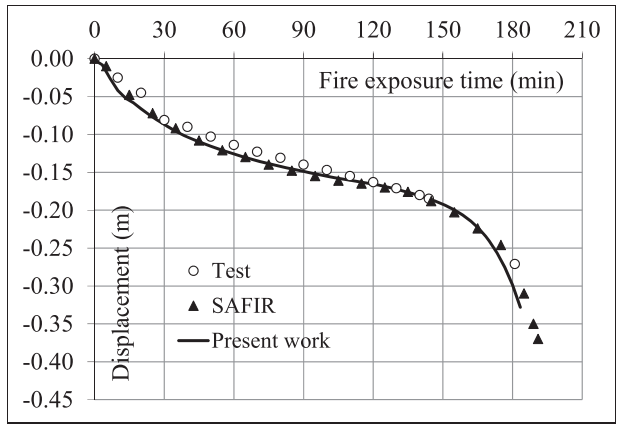

Figure 6. Central displacement of slab tested by Lim and Wade [33].

diameter in both directions. The yield strength of steel was 565 MPa. The reinforcement was considered cold worked and the modified properties for concrete at elevated temperatures were taken into account in accordance with Eurocode 2 [21]. Calcareous aggregate, the lower limit for thermal conductivity and a moisture content of 3% by weight were considered in the analysis. The slab thickness was subdivided into 22 layers.

The results shown in Figure 6 are all consistent and have a higher displacement rate in the first 30 min, a gradual displacement rate thereafter and finally an increase from 150 min until failure. Talamona and Franssen [13] discuss that the high fire resistance of the lightly reinforced slab was attributed to the loads being resisted by tensile membrane action instead of bending action.

Conclusion

This article presents the development of a numerical model for concrete slabs in fire consisting of a shell finite element, a damage constitutive model for concrete with steel reinforcement and the consideration of heat transfer through the thickness of slabs. The damage constitutive model has the significant advantage of using the complete stress–strain relationship for concrete, which differs from other models that are based on failure surfaces and plasticity. The stress–strain relationship in Eurocode 2 [21] was implemented here but can be modified to simulate other types of concrete.

Several calculations have been performed to validate the model. The comparison with experimental tests and numerical results confirms the validity of the approach for reinforced concrete slabs exposed to large transverse displacement.

Further developments may result in changes to the constitutive model necessary to account for the behavior of composite slabs, spalling effects and a better representation of the compressive and tensile behavior of concrete.

Acknowledgments

The authors thank Vallourec-Mannesmann (V&M Tubes do Brasil), CNPq (Conselho Nacional de Desenvolvimento Científico e Tecnológico), FAPEMIG (Fundação de Amparo à Pesquisa do Estado de Minas Gerais) and the research support program for new doctors, PRPq 08-2010, from the Federal University of Minas Gerais, for their financial support.

Funding

This research received no specific grant from any funding agency in the public, commercial, or not-for-profit sectors.

References

1. Newman GM, Robinson JT and Bailey CG. *Fire safe design: A new approach to multi-storey steel-framed buildings*. 2nd edn. The Steel Construction Institute. SCI Publication P288, 2006.
2. Vassart O and Zhao B. *FRACOF, fire resistance assessment of partially protected composite floors*. Engineering Background Document, ANEFORE European Education Program, Luxemburg, 2011.
3. Vassart O and Zhao B. *MACS+, membrane action of composite structures in case of fire*. Engineering Background Document, ANEFORE European Education Program, Luxemburg, 2012.
4. Vassart O, Hawes M and Simms I, et al. *FICEB+, fire resistance of long span cellular beam made of rolled profiles*, Design Guide, 2011.
5. Nizamuddin ZT. *Thermal and structural behaviour of steel-framed buildings in fire*. PhD Thesis, University of California, Berkeley, California, 1976.
6. Bailey CG. *Simulation of the structural behavior of steel-framed buildings in fire*. PhD dissertation, University of Sheffield, Sheffield, UK, 1995.
7. Huang Z, Burgess IW and Plank RJ. Nonlinear analysis of reinforced concrete slabs subjected to fire. *ACI Struct J* 1999; Vol. 96(1): 127–13.
8. Huang Z, Burgess IW and Plank RJ. Modelling membrane action of concrete slabs in composite buildings in fire: I: Theoretical development. *J Struct Eng* 2003; Vol. 129(8): 1093–1102.
9. Huang Z, Burgess IW and Plank RJ. Effective stiffness modelling of composite concrete slabs in fire. *Eng Struct* 2000; Vol. 22: 1133–1144.
10. Lim L, Buchanan A and Moss P. Analysis and design of reinforced concrete slabs exposed to fires. In: *Proceedings of Third International Workshop "Structures in Fire"*, SiF 2004, National Research Center, Ottawa, Canada, 10–11 May, 2004.
11. Lim L, et al. Numerical modelling of two-way reinforced concrete slabs in fire. *Eng Struct* 2004; Vol. 26: 1081–1091.
12. Franssen JM. SAFIR: A thermal/structural program for modeling structures under fire. *Eng J* 2005; Vol. 3rd Quarter: 143–158.
13. Talamona D and Franssen JM. A quadrangular shell finite element for concrete and steel structures subjected to fire. *J Fire Protect Eng* 2005; Vol. 15: 237–264.
14. Elghazouli AY, Izzuddin BA and Richardson AJ. Numerical modelling of the structural fire behaviour of composite buildings. *Fire Safety J* 2000; Vol. 35: 279–297.

15. Elghazouli AY and Izzuddin BA. Analytical assessment of the structural performance of composite floors subject to compartment fires. *Fire Safety J* 2001; Vol. 36: 769–793.
16. Gillie M, Usmani A and Rotter M. A structural analysis of the first cardington test. *J Construct Steel Res* 2001; Vol. 58: 581–601.
17. Newman GM, Robinson JT and Bailey CG. *Fire safe design: A new approach to multi-storey steel-framed buildings*. The Steel Construction Institute, SCI Publication P288, 2000.
18. Bailey CG. Steel structures supporting composite floor slabs: Design for fire. *BRE Digest* 2001; 462.
19. Bailey CG and Toh WS. *Experimental behaviour of concrete floor slabs at ambient and elevated temperatures*. In: *Proceedings of the Fourth International Workshop ''Structure in Fire''*, SiF'06, University of Aveiro, Aveiro, Portugal, 10–12 May, 2006.
20. Tenchev R and Purnell P. An application of a damage constitutive model to concrete at high temperature and prediction of spalling. *Int J Solids Struct* 2005; Vol. 42: 6550–6565.
21. *Eurocode 2: Design of Concrete Structures, Part 1.2: General Rules, Structural Fire Design*. European Committee for Standardization, EN 1992-1-2:2004, 2004.
22. Caldas RB. *Numerical analysis of steel, concrete and composite structures subjected to fire*. PhD Thesis (in Portuguese), Universidade Federal de Minas Gerais, Belo Horizonte, Brazil, 2008.
23. Martha LF and Parente Jr E. An object-oriented framework for finite element programing. In: *Fifth World Congress on Computational Mechanics*, WCCM V, 7–12 July 2002, Vienna, Austria.
24. Sousa JBM Jr and Caldas RB. Numerical analysis of composite steel-concrete columns of arbitrary cross section. *J Struct Eng* 2005; Vol. 131(11): 1721–1730.
25. Huang Z, Burgess IW and Plank RJ. Modelling membrane action of concrete slabs in composite buildings in fire: II: validations. *J Struct Eng* 2003; Vol. 129(8): 1103–1112.
26. Bazant ZP and Oh BH. Crack band theory for fracture do concrete. *Matériaux et Constructions* 1983; Vol. 16(93): 155–177.
27. Pitangueira RLS. *Mechanics of structural concrete including heterogeneity and size effect*. PhD Thesis (in portuguese), Departamento de Engenharia Civil, Pontifícia Universidade Católica do Rio de Janeiro, Rio de Janeiro, Brazil, 1998.
28. Parente E Jr, Holanda AS and Silva SMBA. Tracing nonlinear equilibrium paths of structures subjected to thermal loading. *Comput Mech* 2006; Vol. 38: 505–520.
29. Crisfield MA. *Non-linear finite element analysis of solids and structures. Volume 1: essentials*. Imperial College of Science, Technology and Medicine, London, UK, John Wiley & Sons, 1991.
30. Ghoneim MG and MacGregor JG. Behavior of reinforced concrete plates under combined inplane and lateral loads. *ACI Struct J* 1994; Vol. 91(2): 188–197.
31. Ghoneim MG and McGregor JG. Tests of reinforced concrete plates under combined inplane and lateral loads. *ACI Struct J* 1994; Vol. 91(1): 19–30.
32. Lin TD, et al. Fire test of concrete slab reinforced with epoxy-coated bars. *ACI Struct J* 1989; Vol. 86(2): 156–162.
33. Lim L and Wade C. *Experimental fire tests of two-way concrete slabs*. Department of Civil Engineering, University of Canterbury, Fire Engineering Research Report 02/12, New Zealand, 2002.